https://doi.org/10.1595/205651323X16787270178522 *Johnson Matthey Technol. Rev.*, 2023, **67**, (3), 266–277

JOHNSON MATTHEY
TECHNOLOGY REVIEW

technology.matthey.com

Properties of Additively Manufactured Platinum-Rhodium Alloys

Investigating the feasibility of additive manufacturing for glass fibre bushings

Thilo Becker*, Thomas Gries
Institut für Textiltechnik of the RWTH Aachen University, Otto-Blumenthal-Str. 1, 52066 Aachen, Germany

***Email:** thilo.becker@ita.rwth-aachen.de

PEER REVIEWED

Received 9th December 2021; Revised 3rd January 2022; Accepted 9th February 2022; Online 5th May 2023

Bushings made of platinum-rhodium alloys are a key component in glass fibre production. While bushings have grown in size and functionality since their introduction in the early 20th century, manufacturing constraints still limit their full potential. Both in terms of design and quality, traditional manufacturing methods such as milling, drilling and welding limit the potential of precious metal bushings. The technical feasibility of the use of additive manufacturing for the production of bushings is greatly dependent on the material properties. For the purpose of this work, an additively manufactured alloy consisting of 90 wt% platinum and 10 wt% rhodium (PtRh10) is investigated with regard to density, electrical resistivity, creep performance and the contact angle of E-glass on the PtRh10 samples.

1. Introduction

Glass fibres are inorganic non-crystalline thin filaments that, in their most simple form, date back to ancient Egypt (1). They play a key role in technologies of great commercial importance such as multilayer printed circuit boards (PCBs), composite wind turbine blades and lightweight boats. At a price of approximately €1.1 kg^{-1}, chopped (≤50 mm length) and continuous glass fibres dominate the reinforcement fibre market with a total production volume of approximately 700,000 tonnes in the European Union (EU) in 2018. Including imported glass fibres, the total annual demand for glass fibres within the EU in 2018 was just over 1.05 million tonnes (2). Estimates for the global glass fibre production in 2019 vary between 5 million tonnes and 8 million tonnes (3, 4).

The commercial production of glass fibres dates back to the 19th century. In France, glass fibres were produced as early as 1830 in small volumes and woven to produce garments. In 1908, W. v. Paczinsky produced continuous glass fibres using a platinum vessel, a so-called bushing, for the first time in Hamburg (Germany) (5). As defined by ASTM C162-05, a bushing is "a precious metal or refractory/metal structure with single or multiple hole(s) through which glass flows and is attenuated into fiber(s)" (6). The key role of the bushing is to provide a heated vessel for a glass melt, comprising a multiplicity of openings from which glass fibres can be drawn. **Figure 1** depicts the lower section of a bushing, the so-called tip plate. Commercial production of glass fibres *via* this process began in 1930 in the USA and 1939 in Germany (5). Since that time, the underlying principle of drawing glass filaments from a glass melt through narrow tips (nozzles) in precious metal bushings has remained largely unchanged. The same process is also employed in the production of continuous basalt fibres. The bushing forms a critical part of the glass fibre production process. Typical operating temperatures are between 1150°C and 1500°C, depending on the glass composition. While bushing technology has

© 2023 Johnson Matthey

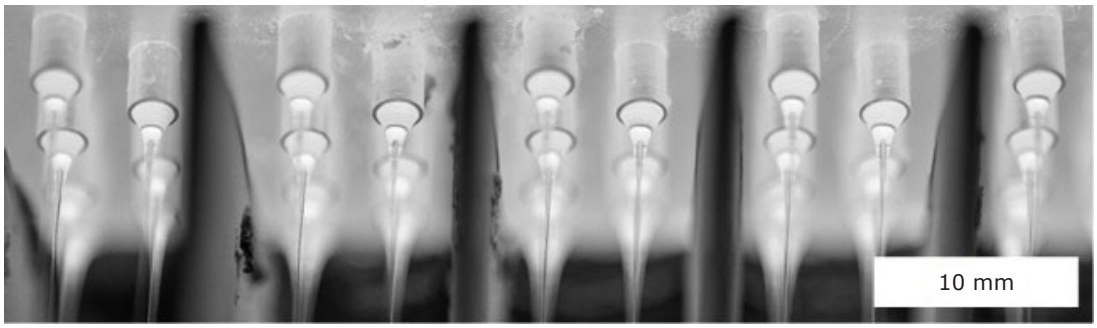

Fig. 1. Section of an operational tip plate of a 203-tip bushing with fin coolers between double rows of tips

advanced with regard to increases in the number of tips and functionality, manufacturing constraints of traditional manufacturing methods such as milling, drilling and welding still limit their full potential both in terms of design and quality.

Manufacturing techniques for bushing tip plates such as deep-drawing and welding feature manufacturing constraints with regard to the design of a bushing, and in particular the complex tip plate of a bushing. Manufacturing the tip plate accounts for approximately 40% of the total manufacturing costs of €12,000–€15,000 for a typical 4000 tip bushing. The conventional production of a bushing is very time-consuming and cost-intensive due to the numerous tips. In addition, every weld seam increases the risk of failure and glass leakage. This must be counteracted by elaborate quality control. The risk of leakage can be reduced by deep-drawing the nozzle plate, but the production of the required tools is very cost-intensive. The additive manufacturing technology shows potential to overcome these deficits, as it enables the production of complex monolithic parts without external weld lines and to a high level of precision. Furthermore, it enables complex design features such as narrow adjacent walls, hollow structures or finely detailed tips which are either impossible to produce through conventional methods or are simply not economical.

Additive manufacturing, also known as '3D printing', is a technology through which parts are produced by adding material, usually layer by layer, to form a desired geometry. The technology emerged in the 1980s, with the first patent in the field of additive manufacturing filed in 1984 by William E. Masters (7). In 2014, the first commercially available additive manufacturing machine for precious metals, the Precious M 080 (EOS GmbH Electro Optical Systems, Munich, Germany), was introduced to the market (8). While initially designated for jewellery production, the new precious metal additive manufacturing systems also show significant potential for industrial processes. Offering great design freedom in three-dimensional space, the process enables geometries and part functionality which can often not be achieved with conventional subtractive manufacturing methods.

Additive manufacturing of PtRh10 alloys is still a relatively new technology. Little work has gone into optimising the material with regard to the relevant material properties for bushings. However, previous work has shown that metal parts manufactured through laser powder bed fusion (LPBF) can be optimised to achieve similar or even superior properties to cast or rolled parts (9, 10). In this present work, three properties of additively manufactured PtRh10 alloys are investigated, namely electrical resistivity, creep performance and the contact angle of E-glass on the PtRh10 samples. By evaluating these properties, the potential of the additive manufacturing technology for the production of glass fibre bushings is evaluated.

The electrical resistivity is critical for bushings, as they are heated through Joule heating, also referred to as resistive heating. The creep performance of the bushing is of great importance for its service life. Particularly with large bushings featuring 2400 tips or more, the large surface area of the tip plate is prone to sagging due to material creep under the hydrostatic pressure (P) of the glass melt, as indicated in **Figure 2**.

In a study conducted by Yang *et al*., the average lifetime of an industrial 2400 tip bushing was analysed. A total of 84 bushings, 14 bushings each from six different furnaces were analysed. An average lifetime of 368 days with a large standard deviation of 114 days was recorded. Despite the lack of essential information such as bushing geometry, material or processing conditions, these figures provide general insights into typical bushing lifetimes (11). Further values available in literature suggest average bushing lifetimes between 250 and 350 days, with mechanical failure due to excessive creep being a common cause of failure (12).

© 2023 Johnson Matthey

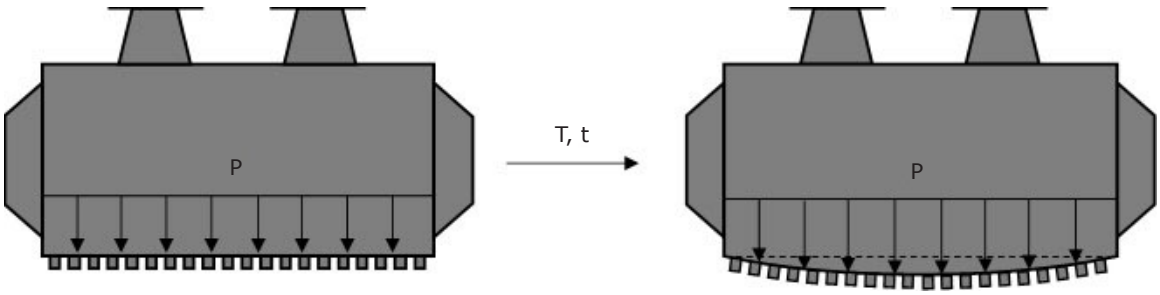

Fig. 2. Schematic of the sagging of a tip plate of a bushing due to the effects of temperature (T), time (t) and pressure (P)

Finally, the contact angle with the glass melt is of great importance for the performance of bushings to enable a stable fibre drawing process and prevent flooding of the tip plate. Flooding describes the phenomenon of molten glass creeping around the tip openings of the bushing, covering large portions or even the entire tip plate. The surface morphology impacts the contact angle between a liquid and a solid, as outlined by Cassie, Baxter and Wenzel (13, 14). The determination of the contact angle of additively manufactured PtRh10 alloys is important as additive manufacturing often leads to rougher surfaces compared to conventional rolled sheet metal, and post-processing of the surfaces is more challenging due to the complex monolithic geometries.

2. Sample Preparation and Methodology

All additively manufactured PtRh10 samples were prepared on an EOS M 100 (EOS GmbH, Germany) additive manufacturing machine by Cookson Precious Metals Ltd (Birmingham, UK). Prior to testing, the rhodium content of the samples was evaluated through non-destructive X-ray fluorescence (XRF) analysis using an ADVANT XP device manufactured by Thermo Scientific (Waltham, USA). The impurities were determined *via* inductively coupled plasma optical emission spectrometry using an iCAP™ ICP-OES 7400 device by Thermo Fisher Scientific. As all additively manufactured PtRh10 specimens used throughout this work were manufactured from the same batch of raw material powder according to the manufacturer, respective impurities are assumed to be constant across various samples. An additional conventionally manufactured creep specimen was also tested with regard to impurities. The XRF and inductively coupled plasma optical emission spectroscopy (ICP-OES) analyses were conducted on solid platinum-rhodium samples rather than the powder feedstock, as the material quality is assumed to be homogenous across the powder and therefore also across the part. The producer of the additively manufactured parts was unable to provide feedstock for analysis.

The density of an additively manufactured PtRh10 cube measuring 10 mm × 10 mm × 10 mm was determined using an AccuPyc II 1340 gas pycnometer made by Micromeritics Instrument Corp (Norcross, USA). 10 volume measurements were conducted through the AccuPyc II 1340 gas pycnometer to account for geometric inaccuracies.

The creep behaviour of additively manufactured PtRh10 samples was evaluated *via* constant load tensile creep tests at a temperature of 1200°C. Additively manufactured 'dog bone' shaped samples measuring 48.4 mm in length, 7 mm in width and 1 mm in thickness were prepared for testing. A central creep portion used to visually determine the elongation of the sample measuring 5 mm in length and 2.9 mm in width is indicated by lateral markers on the samples (**Figure 3**). The creep behaviour was evaluated through the so-called stress rupture time, which describes the time it takes for a sample to fail under a constant stress.

For the determination of the creep rate as well as the rupture time, the PtRh10 samples were inserted into a creep test rig consisting of a furnace, ceramic sample holders and thermocouples. Subsequently the furnace was heated to a temperature of 1200°C at a heating rate of approximately 10°C min^{-1} and once the target temperature was reached, a tensile load of 10 MPa was applied. The deformation over time was recorded optically through a suitable camera (**Figure 4**). A total of three additively manufactured samples were tested with regard to their creep rates and stress-rupture time at a load of 10 MPa at 1200°C. A further three benchmark samples produced through conventional manufacturing were tested.

© 2023 Johnson Matthey

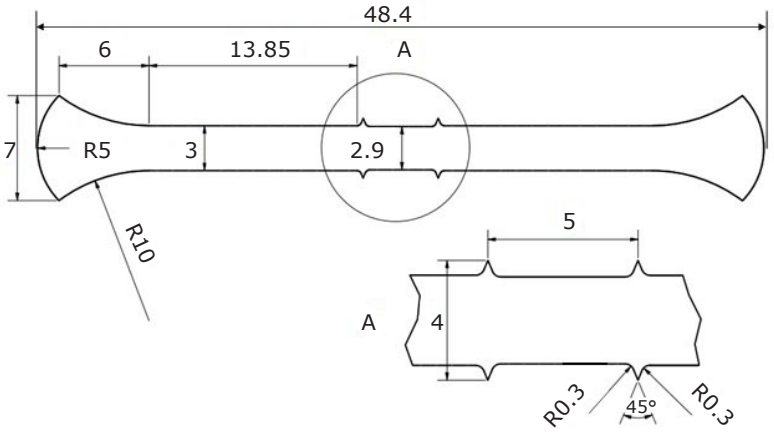

Fig. 3. Geometry of the tensile creep test samples

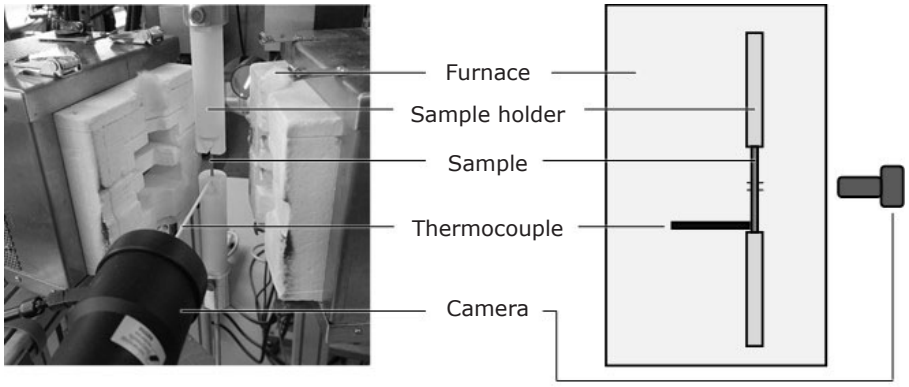

Fig. 4. Overview of the high temperature creep test setup

Table I Chemical Composition of Typical E-Glass[a] According to the Product Datasheet

	SiO_2	CaO	Al_2O_3	B_2O_3	MgO	Fe_2O_3	R_2O	Other
wt%	53.75	20.18	13.87	6.65	3.59	0.28	0.32	1.36

[a]supplied by Unifrax Dongxiang (Songyuan) Co, Ltd (Shenyang City, China)

A similar experimental setup was previously used by Völkl *et al*., allowing for a direct comparison of the creep rates with conventionally manufactured PtRh10 components from this study (15). While standards for creep testing of metals such as ISO 204:2018 or ASTM E139-11(2018) (16, 17) exist, they are not suitable for precious metals. Specified clamping methods, heating systems and temperature monitoring systems are often not compatible with the high-temperature regimes required for testing precious metals.

The contact angle between E-glass and additively manufactured PtRh10 parts was evaluated. The chemical composition of the E-glass is outlined in **Table I**. Glass fragments weighing between 0.01 g and 0.015 g were prepared by crushing E-glass droplets collected from a glass fibre bushing.

The PtRh10 substrates measure 15 mm × 15 mm × 1 mm. Four PtRh10 samples (U1–U4) were analysed in an 'as built' condition without further post-treatment after the additive manufacturing process. A further four samples (B1–B4) were sand-blasted prior to exposure with the glass. In both cases, the surface facing upward during the additive manufacturing process was investigated. Finally, three conventionally manufactured samples (C1–C3) produced by Saxonia Edelmetalle GmbH (Halsbrücke, Germany) were analysed as a benchmark to ensure the comparability of the tests to the data available in literature. Additional polishing was performed on the conventional samples to remove unidirectional surface grooves. Prior to testing, all samples were cleaned with acetone (**Table II**).

© 2023 Johnson Matthey

Table II Overview of the Different Sample Types

	U1–U4	B1–B4	C1–C4
Manufacturing	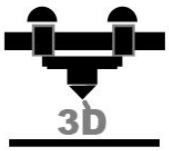 AM	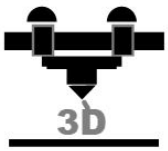 AM	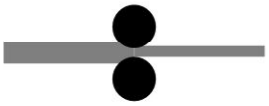 Conventional, rolled
Surface treatment	Acetone	Sand-blasting acetone	Polishing acetone
Dimensions, mm	 15 × 15 × 1	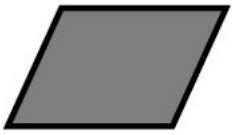 15 × 15 × 1	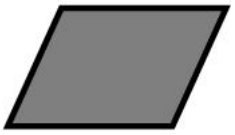 15 × 15 × 1

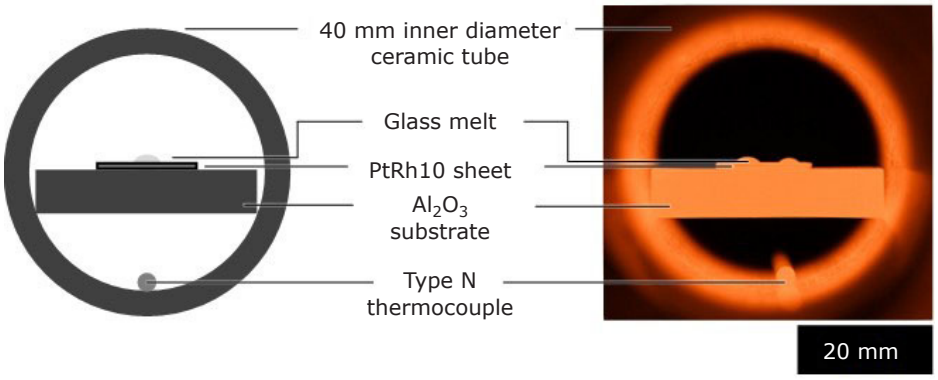

Fig. 5. Schematic and image of the PtRh10 sample within the tube of the tube furnace

A model STF 16-180 tube furnace produced by Carbolite Gero Ltd (Hope Valley, UK) was preheated to 1200°C and an alumina substrate block inserted together with a PtRh10 sample and a glass fragment (**Figure 5**). The furnace temperature was monitored and maintained within ±5°C of the target temperature using a type N thermocouple attached to a RS PRO 1316 digital thermometer (RS Components Ltd, Corby, UK). Images of the shape of the glass on the metal substrate were captured every 10 s for a period of 1 h using a D850™ digital camera with an AF-S Nikkor 28-300 mm f:3.5-5.6G ED VR lens (Nikon Corp, Tokyo, Japan) at a focal length of 300 mm. The captured images were analysed using the ImageJ software developed and published by the National Institutes of Health (Bethesda, USA) (18). More specifically, the LB-ADSA plugin based on the Young-Laplace equation was used to analyse the imaging data [SMM+10]. For analysis, the images were converted to 32-bit black and white images, cropped and rotated for the PtRh10 samples to align horizontally.

Additionally, a detailed surface roughness analysis was conducted using an InfiniteFocusG5 3D focus variation measurement system produced by Alicona Imaging GmbH (Raaba, Austria). Average surface roughness measurements of the arithmetical mean height (S_a) were taken across a central portion of the samples. A 10× magnification lens was used with a specified vertical resolution of 100 nm. A total of nine images were stitched to create a measurement area 4.5 mm × 4.5 mm in size and featuring 27 million measurement points. A Gaussian filter according to ISO 16610-71:2014 (18) was applied through the MeasureSuite 5.3.5 software (Alicona Imaging GmbH) to account for surface curvature.

Three additively manufactured PtRh10 samples measuring 70 mm × 10 mm × 1 mm were produced in different build orientations during the additive manufacturing process (**Figure 6**). No post-treatment of the samples was undertaken besides the removal from the build platform *via* wire electrical discharge machining. An additional three conventionally manufactured samples from

 © 2023 Johnson Matthey

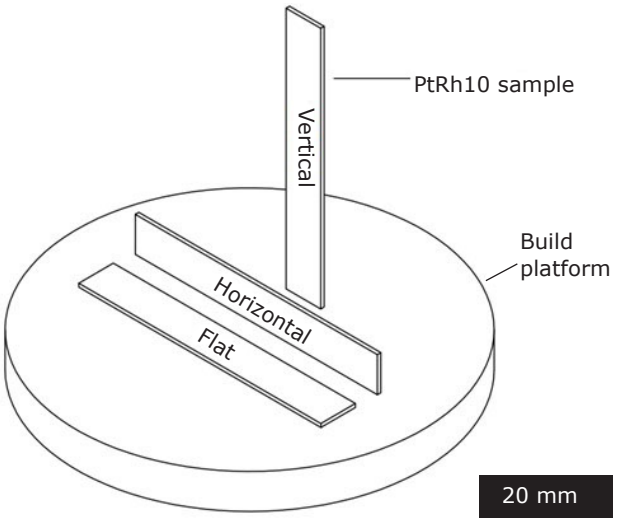

Fig. 6. Build orientation of the different additively manufactured samples

rolled sheet metal of the same geometry were prepared. Based on the work by Silbernagel *et al*., the four-terminal sensing method, also referred to as Kelvin sensing, was applied to determine the electrical resistivity of the samples (19). Using a 5500A Multi-Product Calibrator (Fluke Corp, Everett, USA), a 10 A current was applied through alligator clips at each end of the sample.

The electrical resistivity of a given object with a known geometry can be calculated according to Equation (i) by measuring the electrical resistance, as the resistance is equal to the resistivity of the material times the length and divided by the cross-sectional area:

$$R = (\rho L)/A \quad \text{(i)}$$

where R is electrical resistance in Ω; ρ is electrical resistivity in Ω m; L is length in m; A is cross-sectional area in m^2.

The potential difference across a central portion measuring approximately 50 mm in length was measured using a high-precision 3458A multimeter (Hewlett Packard, USA). The contact probes were manually placed on the samples in a previously marked position along its central axis. An overview of the experimental setup is shown in **Figure 7**. Each additively manufactured sample was measured prior to and after annealing for 1 h at 1260°C. The actual cross-sectional area of each sample was measured to account for inaccuracies during sample preparation when calculating the electrical resistance.

3. Results

3.1 Metallurgical Impurities

Impurities of approximately 0.33 wt% were detected within the additively manufactured sample. A total platinum and rhodium content of 89.83 wt% and 9.84 wt% respectively was measured. The conventionally manufactured sample featured impurities of 0.03 wt% with 89.94 wt% platinum and 10.03 wt% rhodium. An overview of the various impurities is shown in **Table III**. The concentrations of zinc, gold, chromium, ruthenium, silver and tungsten were below the detection threshold of 10 ppm for the conventionally manufactured sample.

3.2 Density

Through an average of 10 volume measurements, a density of 19.942 g cm^{-3} was determined. The measured volume of the cube of 0.9762 cm^3 with a standard deviation of 0.0003 cm^3 deviated slightly from the expected volume of 1 cm^3. Compared with

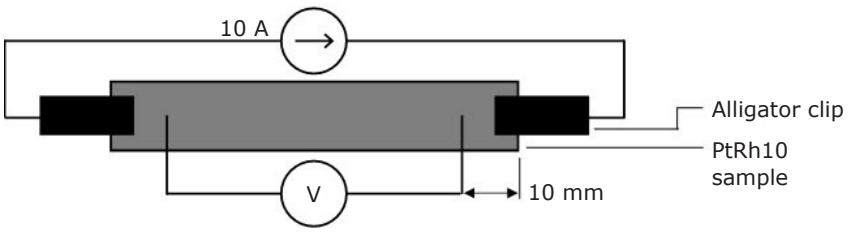

Fig. 7. Schematic of the experimental set-up measuring the potential difference across the PtRh10 samples

Table III Detected Impurities Within the Samples

ppm	Cu	Fe	Zn	Au	Cr	Ir	Ru	Ag	Pd	W	Other
Additive manufacturing	1800	500	460	102	100	60	50	30	29	21	95
Conventional	20	33	–	–	–	78	–	–	94	–	75

© 2023 Johnson Matthey

the reported density of 20.00 g cm^{-3} for PtRh10, a theoretical porosity of 0.29% can be calculated.

3.3 Creep Behaviour

The three additively manufactured samples failed after 23.8 h, 26.1 h and 30.3 h respectively, resulting in a mean rupture time of 26.7 h. A mean elongation at failure of 42.9% with a standard deviation of 4.6% was recorded. An additional three conventionally manufactured samples were tested under the same conditions, resulting in failure times of 63.3 h, 72.0 h and 128.8 h respectively. A mean elongation at failure of 65.7% with a standard deviation of 18.8% was recorded.

3.4 Contact Angle

The surface roughness and surface area of the additively manufactured samples is greatly increased compared to the polished samples. A macroscopic image of the top surface facing the laser beam during the LPBF process of the as-built and sand-blasted samples is depicted in **Figure 8**. This top surface was investigated in the subsequent analysis of surface roughness and contact angle.

Surface defects are present in both additively manufactured samples, with mean measurements of S_a = 5.1 µm and S_a = 5.0 µm respectively for the sand-blasted and as-built surfaces. The polished conventionally manufactured samples feature a mean surface roughness of S_a = 0.2 µm. Additionally, the increase in size of the measured surface compared to the projected surface of 4.5 mm × 4.5 mm was calculated to determine the surface roughness on a smaller scale (**Figure 9**).

The contact angle of the samples was evaluated in a tube furnace. After a rapid decrease in contact angle over the first 5 min within the tube furnace, the equilibrium contact angle is quickly reached. **Figure 10** shows the progression of the contact angle over a period of 30 min for a sand-blasted additively manufactured sample. The curves for all samples, conventional and additive manufacturing, are similar with equilibrium reached after approximately 10 min.

For the samples in 'as-built' condition, a mean contact angle of 35.1° with a standard deviation of 1.1° was measured. The sand-blasted samples showed a slightly increased mean contact angle of 36.2° with a standard deviation of 1.2°, while the conventionally manufactured samples feature a mean contact angle of 43.1° and a standard deviation of 0.7° (**Figure 11**).

According to Wenzel, corresponding roughness factors of 1.12 and 1.10 for the untreated as-built (U) and sand-blasted (B) surfaces can be calculated respectively (13).

3.5 Electrical Resistivity

In the horizontally built samples, a change in both mean resistivity and standard deviation can be observed after annealing (**Figure 12**). Similarly, the vertically built samples show little change in resistivity after annealing, with a mean resistivity of 22.2 µΩ cm both prior to and after annealing (**Figure 12**). Both vertically and horizontally built additive manufacturing samples show a

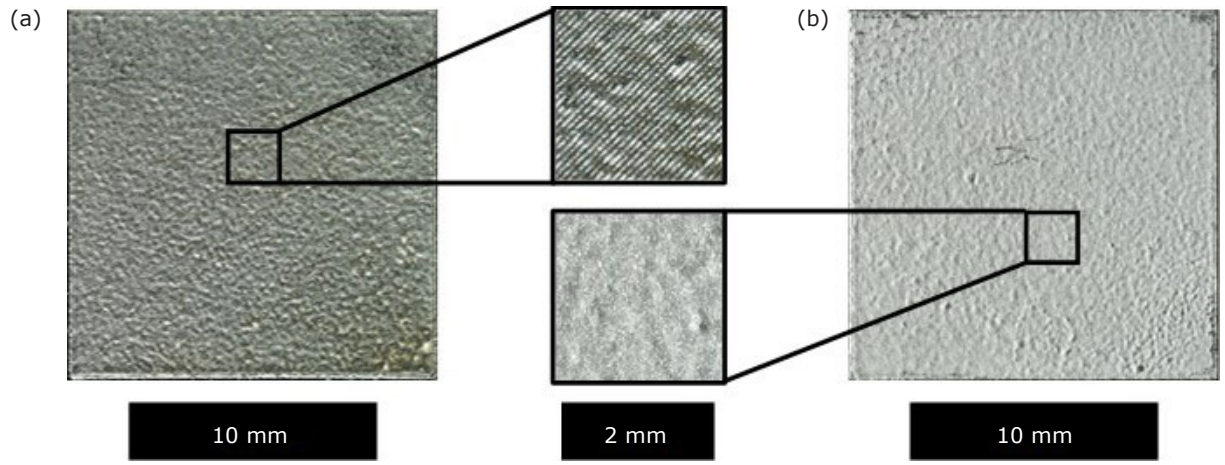

Fig. 8. Surface structure of: (a) as-built; and (b) sand-blasted PtRh10 samples

© 2023 Johnson Matthey

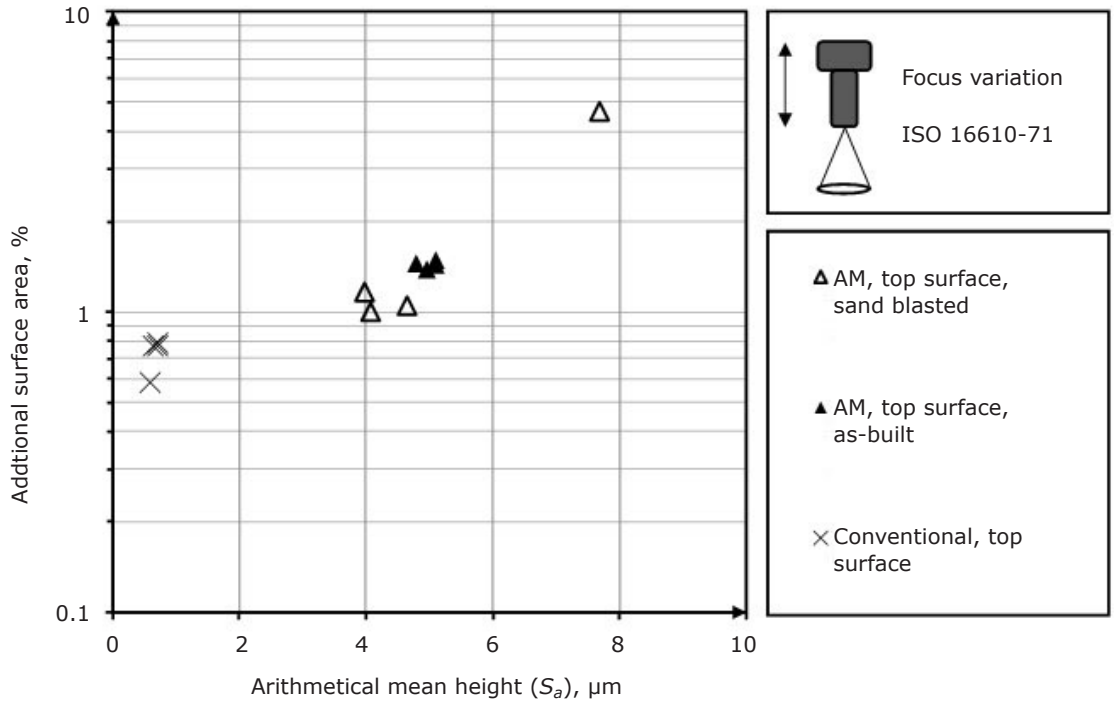

Fig. 9. Additional surface area of the samples plotted on a logarithmic scale against the arithmetical mean height (S_a)

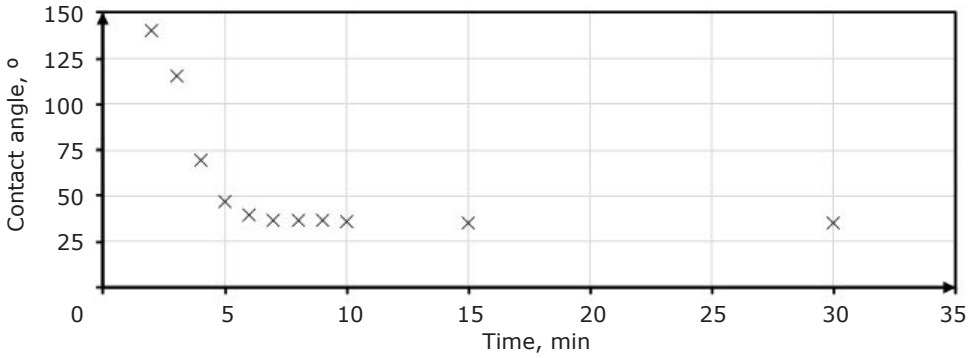

Fig. 10. Measured contact angle between PtRh10 sample and a glass bead over time

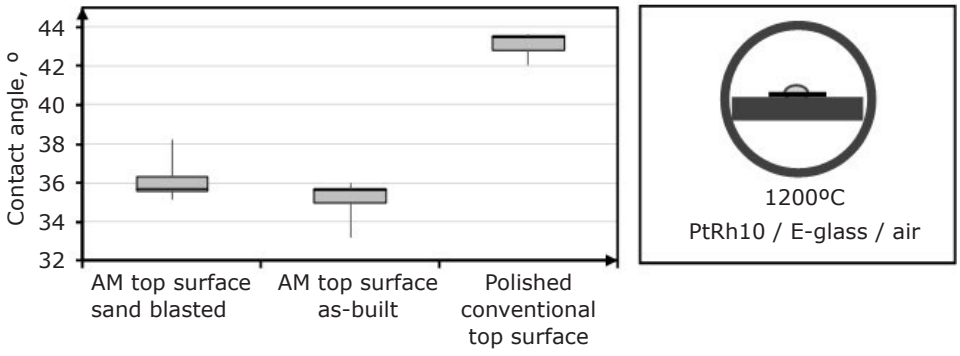

Fig. 11. Box plot diagram of measured contact angles on the various surfaces

higher resistivity than the value of 19.5 µΩ cm measured on the conventionally manufactured samples, which exactly matches the value published by Acken (27). Additional annealing at 1500°C was undertaken on the horizontally built samples, with no measurable change in mean

 © 2023 Johnson Matthey

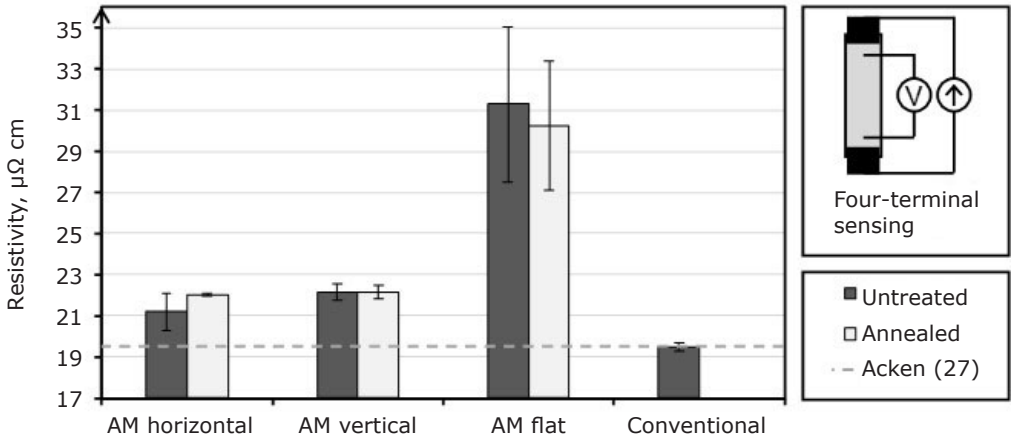

Fig. 12. Electrical resistivity of additively manufactured PtRh10 samples and benchmark value by Acken (27)

resistivity compared to the samples annealed at 1260°C.

The flat additive manufacturing samples feature a mean resistivity of 31.3 µΩ cm and 30.3 µΩ cm and a corresponding standard deviation of 3.8 µΩ cm and 3.1 µΩ cm prior to and after annealing respectively.

4. Discussion

4.1 Metallurgical Impurities

The detected impurities of the additively manufactured samples significantly exceed those investigated in previous creep related studies of platinum-rhodium alloys (20, 21). While all impurities are undesired, zinc is considered to increase creep rates of platinum-rhodium alloys, and typical permissible values in the glass fibre industry are below 50 ppm. Copper is known to reduce the ductility of the alloy, however no concrete data on the effects of concentrations of nearly 2000 ppm were found in the available literature. The source of the impurities is likely from the feedstock, as the production machines are used exclusively for precious metals. The producer of the additively manufactured parts was unable to provide feedstock for analysis to confirm this.

4.2 Density

The reduced volume of the test cube in comparison to the target volume of 1 cm^3 can be attributed to open pores on the surfaces of the cube as well as dimensional inaccuracies during the additive manufacturing and wire cutting process. The porosity of 0.29% is due to a combination of internal voids and vacancies as well as metallurgical impurities.

4.3 Creep Behaviour

The creep behaviour of the additively manufactured samples agrees with data on conventionally manufactured PtRh10 wire published by Trumić *et al*. (21). Though no detailed analysis of impurities is provided in said studies, purities of 99.95% for platinum and 99.5% for rhodium are quoted as well as unquantified impurities of palladium, silver, gold, bismuth, antimony, arsenic and copper. When compared to other studies such as those published by Völkl *et al*. and Hamada however, the observed rupture times are significantly shorter (**Figure 13**) (15, 22). The short rupture times of the additive manufacturing specimens can therefore be attributed to the impurities of 0.33 wt%.

4.4 Contact Angle

The contact angle between an E-glass melt and the additively manufactured platinum-rhodium samples is reduced compared to conventionally manufactured polished samples. The polished samples further show a larger contact angle when compared to the value of 41° published by Selman *et al*. at a temperature of 1200°C (26). As outlined by Selman *et al*. when comparing their own findings to previous studies, this can at least partially be explained by different states of oxidation of the platinum-rhodium alloys. For the purpose of this work however, it can clearly be observed that the PtRh10 samples with a rougher additively manufactured surface show a smaller contact angle with E-glass droplets under air than

© 2023 Johnson Matthey

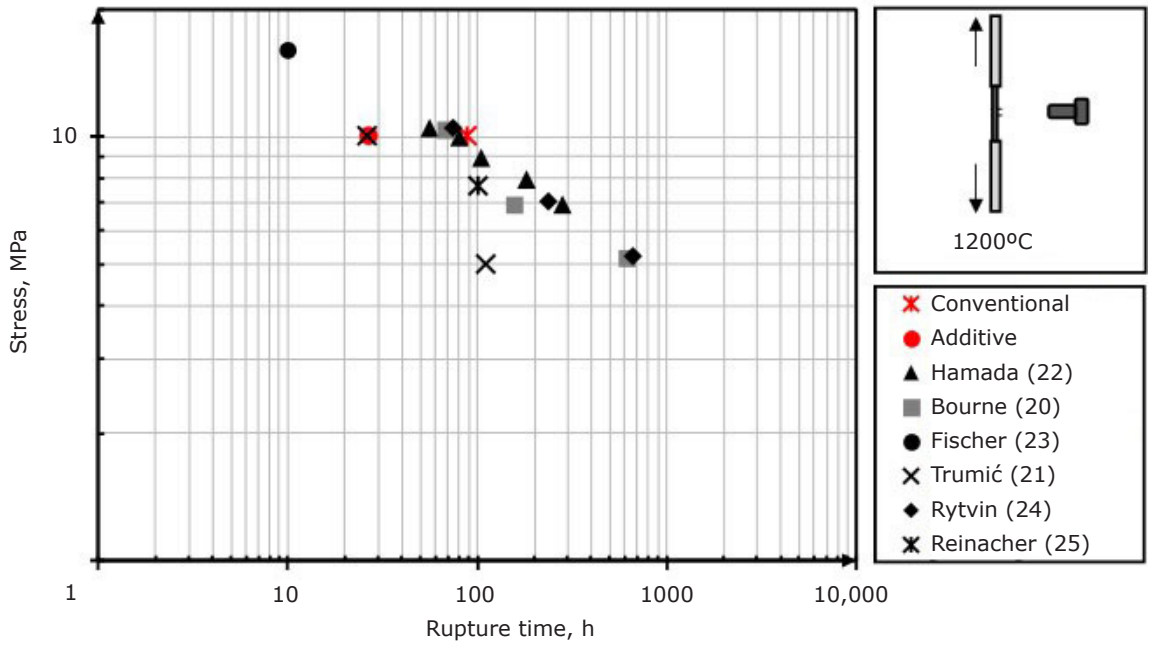

Fig. 13. Stress-rupture time of the mean values of the present study as well as results from previous studies with conventional PtRh10 (21–25)

conventionally manufactured polished surfaces. More specifically, the sand-blasted surfaces (B) show a 16.0% smaller surface angle in comparison to the conventional polished samples.

4.5 Electrical Resistivity

The annealing appears to have little effect on the measured resistivity of the samples. When comparing the resistivity of the horizontally built samples before and after annealing, no statistically significant difference could be detected by applying a two-tailed t-test (p = 0.3). The difference in the mean values is likely due to a measurement error, as two of the three measurements prior to annealing are within 1% of the measured resistivity after annealing. Omitting this outlier, the mean resistivity is 21.8 µΩ cm prior to annealing and 22.0 µΩ cm after annealing for the horizontally built samples.

The flat additive manufacturing samples are outliers within this series, with a mean resistivity of 31.3 µΩ cm and 30.3 µΩ cm and a corresponding standard deviation of 3.8 µΩ cm and 3.1 µΩ cm prior to and after annealing respectively. This is likely due to remains of the support structure from the additive manufacturing process attached to the bottom of the samples (**Figure 14**).

With the supplier of the parts unable to execute a clean cut along the border between the support structure and the sample, the lower surface of the flat samples features an irregular surface. This causes problems during the contacting of the samples through the crocodile clips. Furthermore, the true cross-sectional area is therefore smaller than the product of the width and thickness of the sample, leading to measurement errors. All as-built and tempered additively manufactured samples show a higher resistivity than the reference value of 19.5 µΩ cm. As outlined by Silbernagel *et al.*,

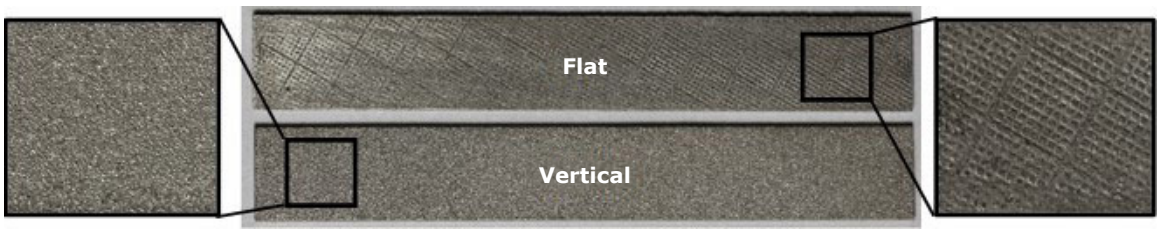

Fig. 14. Comparison of the surfaces of additive manufacturing parts built in the flat and vertical orientation, showing remains of the support structure on the flat samples (right)

© 2023 Johnson Matthey

disruptions in the atomic lattice structure of pure metals govern the electrical resistance of pure solid metals. These disruptions are generally grain boundaries, vacancies or voids (19). For alloys, such as the PtRh10 alloys present in this study, such disruptions are typically caused by elements other than the main elements of the alloy. The higher resistivity of the additively manufactured samples is therefore likely due to a combination of internal vacancies or voids and the metallurgical impurities. The annealing has little effect on the measured resistivity. The observed increase in resistivity after annealing in the horizontal samples is likely due to a measurement error in the untreated samples, as two out of three measurements are within a 1% margin prior to and after annealing.

5. Conclusion

The metallurgical impurities within the additively manufactured samples are outside of common standards within the glass fibre industry. The high level of impurities leads to reduced stress-rupture-times, highlighting the requirement for raw materials of consistently high quality to enable the industrial use of additive manufacturing for the production of glass fibre bushings. The density of the additively manufactured parts is within <0.5% of conventionally manufactured parts and generally suitable for use in bushings. For the manufacturing of bushings, the higher electrical resistivity of the additively manufactured components is generally advantageous, as lower currents are required in the electrical heating system. Components of the electrical heating system such as busbars can be reduced in size with lower currents and system losses reduced.

Finally, the 16% smaller contact angle of the rougher additively manufactured surfaces with E-glass melt is generally disadvantageous with regard to bushing performance. The real-life implications of this however can only be determined through experimental trials investigating the fibre forming and flooding behaviour of additively manufactured tip plates and bushings.

In summary, this work provides a first overview of the feasibility of additive manufacturing for glass fibre bushings by shining a light on the most relevant material properties. Further work is recommended to increase material feedstock quality and additive manufacturing parameters to optimise these properties, and the creep performance in particular.

References

1. K. L. Loewenstein, "The Manufacturing Technology of Continuous Glass Fibres", 2nd Edn., Elsevier, Amsterdam, The Netherlands, 1983
2. Commission Implementing Regulation (EU) 2020/379, *Official J. Eur. Union*, 2020, **63**, (L69), 14
3. S. Mazumdar, 'The Glass Fiber Market', *Composites Manufacturing*, Winter 2021, pp. 18–19
4. T. Becker, M. Haag, T. Gries, D. Pico, C. Wilms, G. Seide, R. Kleinholz and H. Tiesler, 'Fibers, 12. Glass Fibers', in "Ullmann's Encyclopedia of Industrial Chemistry", Wiley-VCH Verlag GmbH and Co KGaA, Weinheim, Germany, 2022
5. R. Teschner, "Glasfasern: 2. Auflage", Springer-Verlag GmbH, Berlin, Germany, 2019 (in German)
6. 'Standard Terminology of Glass and Glass Products', ASTM C162-05, ASTM International, West Conshohocken, USA, 2015, 16 pp
7. W. E. Masters, 'Computer Automated Manufacturing Process and System', *US Patent* 4,665,492; 1987
8. B. Krassenstein, 'EOS & Cooksongold Team to Launch the PRECIOUS M 080 Jewelry DMLS 3D Printer', 3DR Holdings, New York, USA, 15th September, 2014
9. I. Raffeis, U. Vroomen, F. Adjei-Kyeremeh, D. Großmann, H. Hammelrath, E. Westhoff, S. Bremen, D. Boscolo Bozza and A. Bührig-Polaczek, *Materialwiss. Werkstofftech*., 2020, **51**, (4), 432
10. J.-R. Zhao, F.-Y. Hung, C.-S. Lu and I.-C. Lai, *Adv. Eng. Mater*., 2021, **23**, (6), 2001366
11. C.-L. Yang and K.-T. Yu, *J. Fail. Anal. Preven*., 2013, **13**, (5) 521
12. H. Stiller, 'Material Intensity of Advanced Composite Materials: Results of a Study for the Verbundwerkstofflabor Bremen eV', Wuppertal Papers, No. 90, Wuppertal Institute for Climate, Environment, Energy gGmbH, Wuppertal, Germany, 1999, 38 pp
13. R. N. Wenzel, *Ind. Eng. Chem*., 1936, **28**, (8), 988
14. A. B. D. Cassie and S. Baxter, *Trans. Faraday Soc*., 1944, **40**, 546
15. R. Völkl, D. Freund and Fischer, *J. Test. Eval*., 2003, **31**, (1)
16. 'Metallic Materials – Uniaxial Creep Testing in Tension – Method of Test', ISO 204:2018, International Organization for Standardization, Geneva, Switzerland, 2018, 53 pp
17. 'Standard Test Methods for Conducting Creep, Creep-Rupture, and Stress-Rupture Tests of Metallic Materials', ASTM E139-11, ASTM International, West Conshohocken, USA, 2018, 14 pp

 © 2023 Johnson Matthey

18. 'Geometrical Product Specifications (GPS) – Filtration – Part 71: Robust Areal Filters: Gaussian Regression Filters', ISO 16610-71:2014, International Organization for Standardization, Geneva, Switzerland, 2014, 20 pp
19. C. Silbernagel, I. Ashcroft, P. Dickens and M. Galea, *Addit. Manuf.*, 2018, **21**, 395
20. A. A. Bourne and A. S. Darling, *Platinum Metals Rev.*, 1963, **7**, (2), 42
21. B. Trumić, L. Gomidželović, S. Marjanović, A. Ivanović and V. Krstić, *Mat. Res.*, 2017, **20**, (1), 191
22. T. Hamada, 'High Temperature Creep of Platinum and Its Alloys', Dissertation, Department of Physical Science, Osaka University, Japan, January, 1998, 87 pp
23. B. Fischer, A. Behrends, D. Freund, D. F. Lupton and J. Merker, *Platinum Metals Rev.*, 1999, **43**, (1), 18
24. E. I. Rytvin, "Heat Resistance of Platinum Alloys", Ore and Metals Publishing House, Moscow, Russia, 1987
25. G. Reinacher, *Platinum Metals Rev.*, 1962, **6**, (4), 148
26. G. L. Selman, M. R. Spender and A. S. Darling, *Platinum Metals Rev.*, 1965, **9**, (4), 130
27. J. S. Acken, *Bur. Stand. J. Res.*, 1934, **12**, (2), 249

The Authors

Thilo Becker works as a research associate and group leader of the inorganic fibres research group at the Institut für Textiltechnik (ITA) of the RWTH Aachen University, Germany. His current research focuses on glass fibre production technology. In recent years, he has driven forward the industrialisation of additive manufacturing technology for the production of glass fibre bushings.

Thomas Gries studied at the RWTH Aachen University. He holds a diploma in mechanical engineering and economics and a doctorate in mechanical engineering. From 1995 to 2001, he worked at Lurgi Zimmer AG, Frankfurt am Main, Germany, at the Department of Technologies for Fibres & Textiles in leading positions. From April 2001 onwards, he is Director of the ITA of RWTH Aachen University.

 © 2023 Johnson Matthey